Kaguya Gamma-Ray Spectrometer (KGRS): Calibrated Spectra Data Processing

N. Yamashita and T. H. Prettyman
Planetary Science Institute

Part of the Kaguya Gamma-Ray Spectrometer calibrated spectra data set
Version 1.0, 14-Jan-2020

Introduction

This document provides an overview of data processing for the JAXA Kaguya Gamma-Ray Spectrometer (KGRS). The data are part of the Planetary Data System (PDS), Kaguya Gamma-Ray Spectrometer Calibrated spectra. The time series spectrum data, with an accumulation interval of 17 s, are archived as ASCII files for each science phase in the lunar orbit. The detailed structures of the archived data files are described in the corresponding label files. The methods used to correct and calibrate the KGRS spectra recorded as a Calibrated product are described here. These follow the approach developed for the analysis of NASA's Lunar Prospector, 2001 Mars Odyssey, and Dawn missions [e.g., *Lawrence et al.*, 2004; *Prettyman and Feldman*, 2012; *Prettyman et al.*, 2004a; 2011].

Mission

The Selenological and Engineering Explorer (SELENE) mission by JAXA consisted of three satellites, a main orbiter named "Kaguya" and two daughter orbiters Relay Satellite and VRAD Satellite, named "Okina" and "Ouna," respectively, after characters in a Japanese fairy tale. The three satellites were launched on Sep. 14, 2007 Japan Standard Time (JST) by the H-IIA rocket from the Tanegashima Space Center, Japan. After separation of the daughter orbiters, Kaguya orbiter was successfully inserted to the lunar orbit on October 4, 2007 JST [*Kato et al.*, 2010].

The SELENE mission carried 14 scientific instruments and one public outreach instrument to the Moon. One of them was the Gamma-Ray Spectrometer, which was deck-mounted on the Kaguya satellite. It employed a large-volume high-purity germanium (HPGe) detector as a main detector, surrounded by a horse-shoe shaped BGO detector and a curved plastic scintillator as anti-coincidence detectors [*Hasebe et al.*, 2008]. This configuration of detectors enabled to suppress background and Compton-scattered gamma-ray events as well as the contribution from high-energy charged particles. The HPGe crystal was cooled by a Stirling mechanical cooler to below 90 K during measurement. Prior to launch, the energy resolution of KGRS's HPGe detector was approximately 0.6% or 4 keV full width at half maximum (FWHM) at 662 keV. See Table 1 for variations in energy resolutions measured in the vicinity of the Moon.

The output of the preamplifier of KGRS's HPGe detector was split into to two main amplifiers with different gains to acquire two energy spectra of gamma rays simultaneously. One is the high-gain

spectrum covering approximately from 0.15 to 3.2 MeV for better peak analyses with the emphasis on radioactive elements. The other is the low-gain spectrum covering approximately from 0.15 to 13 MeV for the full coverage of lunar gamma rays as well as gamma-ray burst phenomena. The pulse heights from both main amplifiers were digitized by a common analog-to-digital converter (ADC) consecutively with the output of 8192 channels. The KGRS had a fixed accumulation interval of 17 s [*Kobayashi et al.*, 2013].

The KGRS measurement of lunar gamma rays consists of three epochs or "Periods" (see Table 1). In Period 1, which lasted from December 2007 through February 2008, the high voltage (HV) applied to the HPGe crystal was 3.1 kV and the Kaguya satellite was in the circular polar orbit with the nominal altitude of 100 km. Period 2 started in July 2008 after KGRS's recovery from HV anomaly. The HV applied was lowered to 2.5 kV while the orbit and altitude were preserved at 100 km. In the beginning and the end of Period 2, the Kaguya satellite was flipped and KGRS faced deep space to measure background gamma rays from the spacecraft on July 4, and December 11 through 12, 2008 UTC. The spectra acquired during the background measurements can be identified using the "background_observation" flag included in the spectrum files, as well as the pointing information of the spacecraft included in the Ephemeris, Pointing, and Geometry (EPG) data file [*Prettyman and Yamashita*, 2020]. Following the second background measurement, the HPGe crystal was annealed for 48 hours at > 80 ℃ to restore its energy resolution that had been degraded due to the exposure to the high-energy particles in space. Period 2 ended in December, 2008 for preparation of Kaguya's descent to lower altitude. After successful descent to the lower, elliptical polar orbit at the nominal altitude of 30 × 50 km with the perilune near the south pole, Period 3 started in February, 2009 with the HV of 2.5 kV. Period 3 ended on May 28, 2009. The SELENE mission concluded when the Kaguya satellite had a controlled crash to the nearside of the lunar surface on June 11, 2009 JST. Initial results based on the KGRS data were published elsewhere [e.g., *Yamashita et al.*, 2010; 2012].

Table 1 Summary of the KGRS Calibrated spectrum data archived at PDS. The background measurements are included in the Period 2 data file. Energy resolution of the HPGe detector is expressed as the FWHM of the 1461 keV gamma ray from ^{40}K [*Kobayashi et al.*, 2013].

Epoch	Start date	End date	# of spectra	HV	Energy resolution	Nominal altitude
Period 1	2007-12-14	2008-02-16	264544	3.1 kV	6–10 keV	100 km
Period 2	2008-07-04	2008-12-15	541419	2.5 kV	12–18 keV	100 km
Period 3	2009-02-10	2009-05-28	527736	2.5 kV	6–7 keV	30×50 km

Methods

The data processing procedures to produce the KGRS Calibrated spectra are as follows.

1. Correction for Differential Non-Linearity

The pulse height of output signals from the HPGe detector is analyzed and digitized by the ADC. Each channel of the ADC has slightly variable widths, causing certain channels to be slightly more likely to count an event while others less likely (see the raw spectrum in Fig. 1). This is called the differential non-linearity (DNL) of ADC and needs to be corrected [*Prettyman et al.*, 2011].

First, there are 1-ch-wide spikes in the raw spectra found every 256 channels with intermediate amplitudes and every 512 channels with high amplitudes. These spikes were removed by substituting the

spikes with the average counts from the adjoining channels. Then, an examination of the relatively flat regions of spectra acquired over long integration times indicates that the DNL pattern repeats itself every 1024 channels. Consequently, the ratios between the raw and spectrally smoothed spectrum were taken for each of the 1024-ch-wide segments, excluding regions near gamma-ray peak tops (Fig. 1). The average of the segments was repeated from 0 to 8181 ch to derive the DNL correction factor. We applied this factor (shown in Fig. 2) to each of the time-series spectrum to remove the DNL artifacts. The average value for the DNL factors is 0.9998, which contributes to preserve the overall counts in spectra.

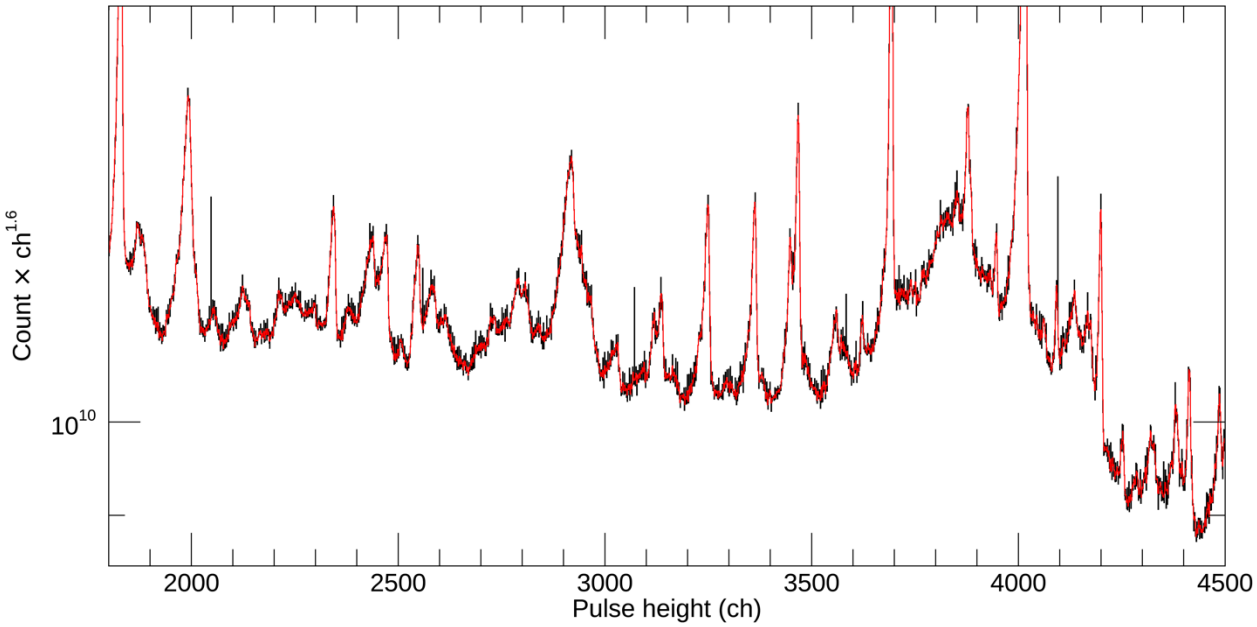

Fig. 1 A raw HPGe low-gain spectrum (black) exhibiting the 1-ch-wide differential non-linearity (DNL) and its spectrally smoothed spectrum (red).

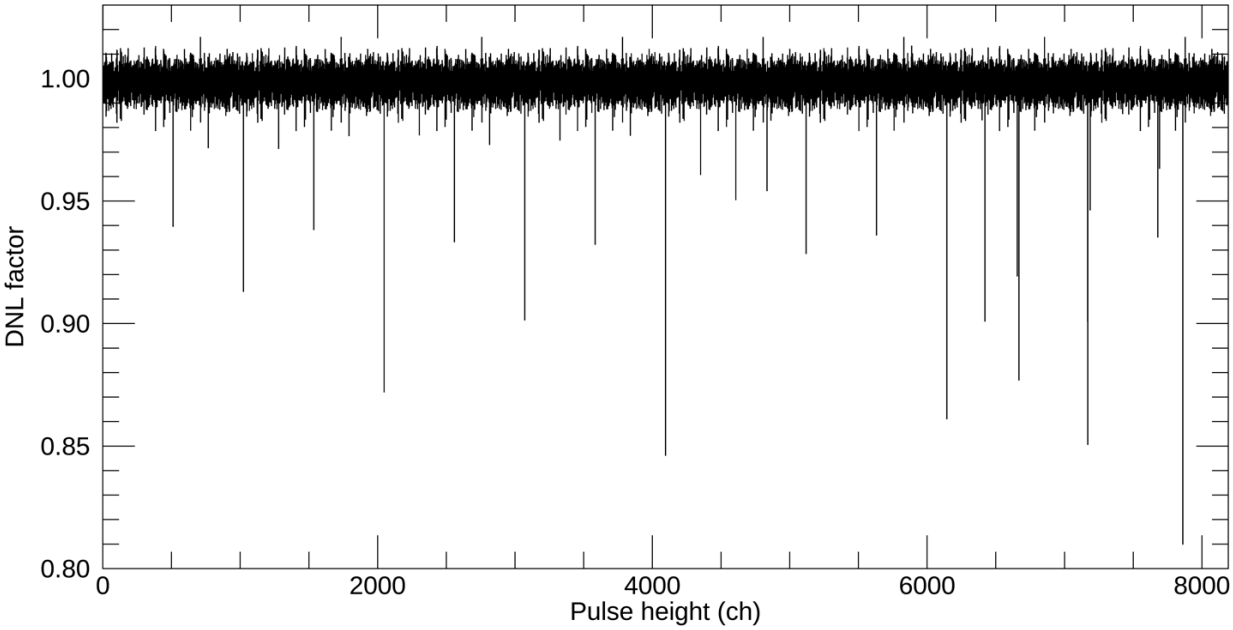

Fig. 2 The differential non-linearity (DNL) factor derived for the KGRS spectra.

2. Determination of Peak Centroids

The gain of the HPGe detector signal is sensitive to the surrounding environment and detector settings such as temperature, intensities of galactic cosmic rays, or HV. Consequently, the gain changed continuously throughout the mission. Temporal changes in the total gain or peak centroid positions in time-series spectra will cause apparent degradation of energy resolution of cumulative spectra, which leads to lower signal-to-noise ratio, poorer elemental identification, and larger spatial resolution. Therefore, it is crucial to correct each and every time-series spectrum to the same gain and offset prior to spectral accumulation for the optimal analysis of planetary gamma-ray spectra.

Temporal variations of centroid channels of the distinct gamma-ray peaks found in HPGe spectra were determined as a proxy for the gain and offset. The peaks used in the analysis of the high-gain spectra were: annihilation 511 keV, Al 1014 keV, Ge 1117 keV, Mg 1369 keV, K 1461 keV, Al 1809 keV, Th 2615 keV, Al 2754 keV. For the low-gain spectra, peaks of annihilation 511 keV, Al 1014 keV, Ge 1117 keV, Mg 1369 keV, K 1461 keV, Al 1809 keV, Th 2615 keV, Al 2754 keV, Si 3539 keV, Si 4934 keV, O 5107 keV, O 5618 keV, O 6129 keV, Fe 7120 keV, Fe 7631 keV, and Al 7724 keV were used (Fig. 3). The centroids were determined by taking the second derivatives using Mariscotti's algorithm, after removal of the power-law continuum [*Mariscotti*, 1967; *Prettyman et al.*, 2011].

Prior to applying the Mariscotti's algorithm each spectrum was temporally smoothed. This is because each time-series spectrum is relatively sparse and contains many channels with low counts or even zero. Therefore we need to take an average of each channel over some period of time. This temporal smoothing is realized by taking the boxcar, central moving average of counts in each channel over variable number of time-series spectra, depending on statistics of the peak of interest. The gain is expected to change

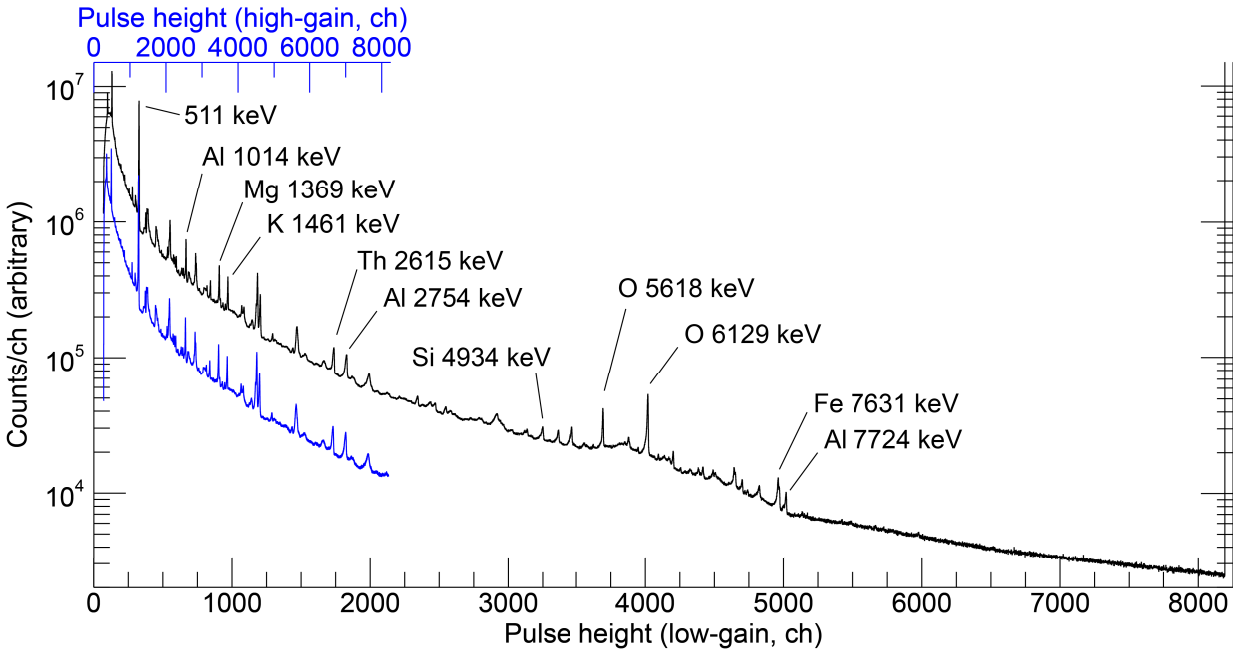

Fig. 3 Uncorrected low-gain (black, x-axis on bottom) and high-gain (blue, x-axis on top) spectra of gamma rays acquired by the KGRS. Some of the distinct peaks are labeled with a source element and gamma-ray energy. Note the low-gain spectrum has the channel width of 1.6 keV/ch and that of the high-gain is 0.4 keV/ch.

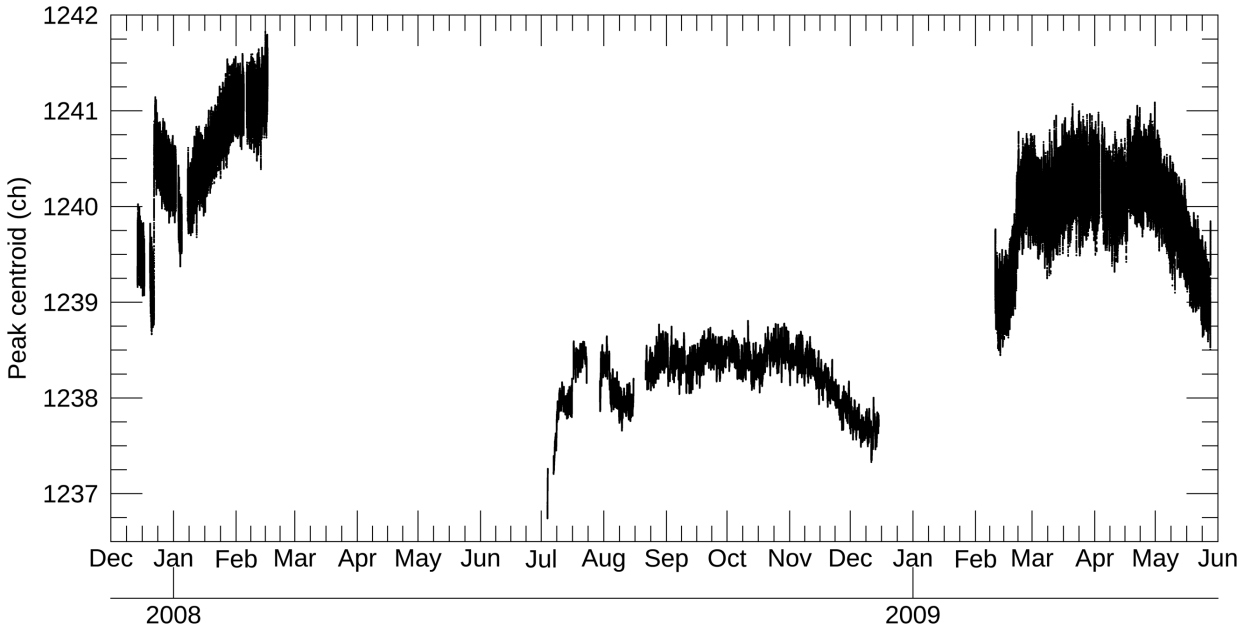

Fig. 4. Temporal variations of centroids for the 511 keV annihilation peak in the high-gain spectra determined by the Mariscotti's algorithm.

relatively slowly with time. In rare cases for low count-rate spectra when these long smoothing windows were statistically insufficient, doubled temporal smoothing windows were used to overcome the statistical uncertainty. The temporal variation of centroids for the annihilation peak at 511 keV is presented in Fig. 4.

3. Gain Correction and Energy Calibration

The temporal variations of the peak centroids were fitted against their reference energies (listed above) to correct all of the time-series spectra to the same gain and offset. Several fitting schemes, including linear and quadratic ones, have been tried. We confirmed that a quadratic regression between the peak centroids and the reference energies give smaller absolute deviations of the peak energies as well as smaller relative deviations among the observation phases than a linear regression.

Using the regression line, the raw channel counts were converted to corrected channel counts with each new pulse height channel having an equivalent energy of *gain_coefficient* × corrected channel number + *offset_coefficient* (keV) [*Lawrence et al.*, 2004; *Prettyman and Feldman*, 2012; *Prettyman et al.*, 2004a; 2004b; 2011]. We calibrated the spectra so that *gain_coefficient* is 0.4 for high-gain and 1.6 for low-gain spectra, and *offset_coefficient* is 0 (zero) for all of the corrected spectra (Fig. 5). The procedure preserves the counts in a spectrum as long as the original channel is not cut off at the upper or lower boundary of the new spectrum following gain correction. Note that the last channel (8191th channel out of 0-8191-ch histogram) in each uncorrected histogram contains a very large number of events that overflowed the range of the ADC (Fig. 5). These overflow counts were eliminated by substituting 8190th-ch values to 8191th ch to avoid the artifacts that otherwise appear in channels around 8060-8191 in the resulting gain-corrected spectra.

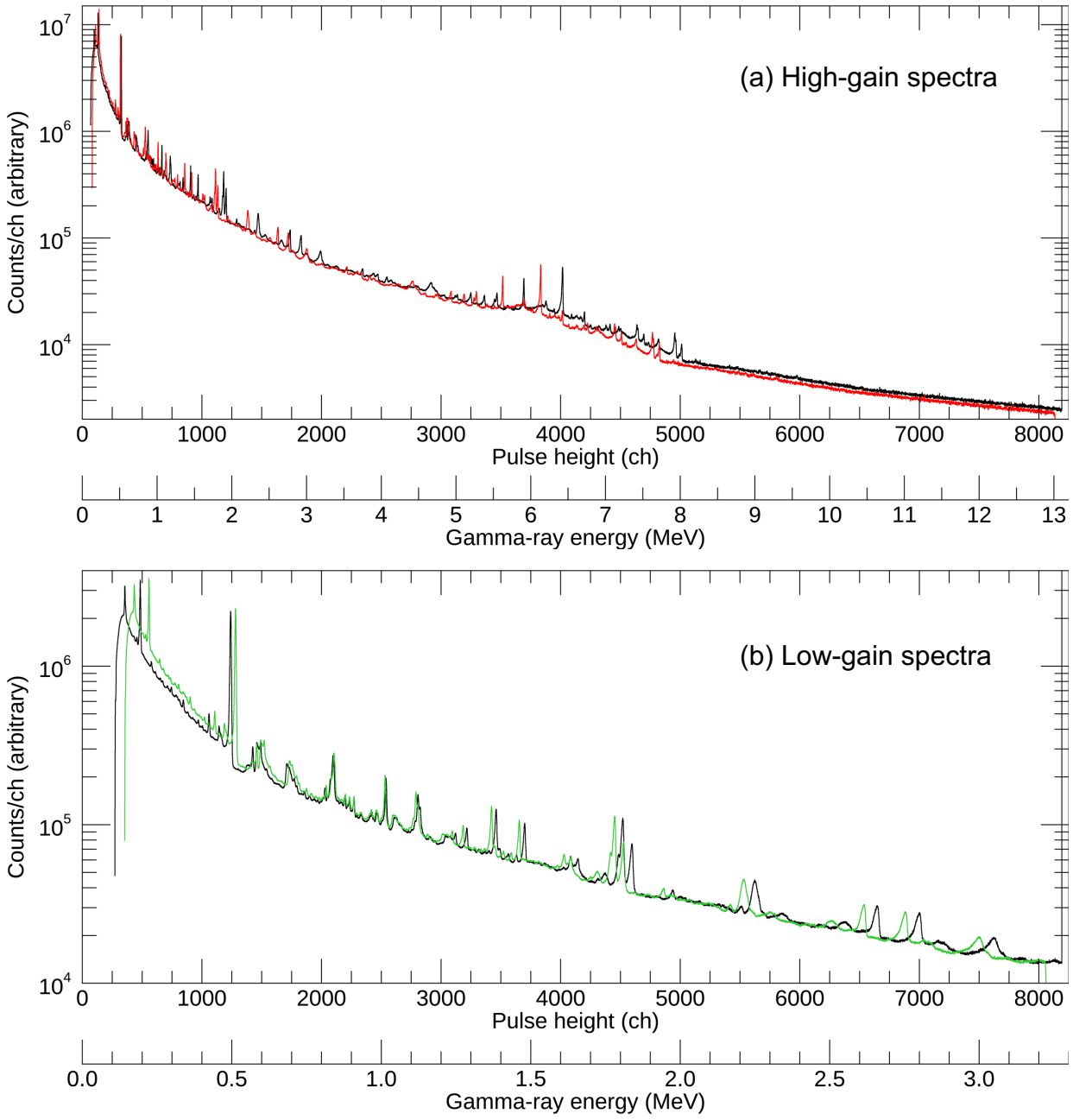

Fig. 5 Corrected (red, green) and uncorrected (black) energy spectra of gamma rays acquired by KGRS. The high-gain spectra are on top (a) and the low-gain spectra are on the bottom (b). An energy scale for each of the corrected spectrum is also appended. The DNL artifacts were removed from the uncorrected spectrum. The overshoot count at 8191th channel in the uncorrected spectrum was removed during the correction processes.

As a result of gain correction, the corrected channel counts now contain floating numbers, because many of raw counts were subdivided and distributed to multiple new channels. As mentioned above, each HPGe raw spectrum is sparse and the newly distributed corrected counts can also be very small in number, but not zero. Such very small decimal values create abnormal shapes in a histogram when accumulated over

time and expressed with its y-axis in logarithm scale. These artifacts of round-off errors were dubbed "cathedral artifacts" after the spectral shape.

To remove such artifacts, the corrected counts were converted back to integers while the total counts in the spectrum were conserved. This was realized by generating a uniform random number ranging 0 to 1 to be compared with a decimal in each channel. If the decimal is greater than the generated random number, then the count in the channel gets rounded up, while if the decimal is smaller, then the count gets rounded down. Consequently, the smallest count (other than zero) that appears in the cathedral-removed spectrum is now 1.

4. Filtering of invalid events

Not all spectra from the raw data set are suited for the elemental analysis of the lunar surface, because some of the spectra were obtained during the solar energetic particle events or the detector settings such as HV were not optimal. These "invalid" events were excluded from the Calibrated data set. The criteria for identifying valid events are mainly based on the following three categories. The rest are filtered out as invalid events.

1) The HV was fully applied to the HPGe detector and anti-coincidence shield detectors. The "full" HV for the HPGe is 3.1 kV for Period 1, and 2.5 kV for Periods 2 and 3. Spectra acquired within 1 minute of the end of HV ramp-up or start of HV ramp-down are considered as invalid.
2) The instrument is fully configured as the Ge data acquisition mode.
3) Scaler values, especially dead times of the instrument, are within the proper ranges. This criterion is slightly loosened during the background measurements in Period 2 because during these times the counting rates were significantly lower.
4) Spectral shape of the HPGe signal is normal. In some cases, HPGe spectra had abnormal shapes or counts, indicating possible data glitches.

Acknowledgements

This work is supported by the NASA under Grant No. NNX16AG54G issued through the Planetary Data Archiving, Restoration, and Tools Program (PDART), Research Opportunities in Space and Earth Sciences (ROSES) 2015. We appreciate the support provided by the PDS Geosciences Node in archiving the data set. We thank reviewers for their valuable contributions to the revision of this manuscript and data set.

References

Hasebe, N., N. Yamashita, O. Okudaira*, et al.* (2008), The high precision gamma-ray spectrometer for lunar polar orbiter SELENE, *Adv. Space Res.*, *42*(2), 323-330, doi:10.1016/j.asr.2007.05.046.

Kato, M., S. Sasaki, Y. Takizawa*, et al.* (2010), The Kaguya Mission Overview, *Space Science Reviews*, *154*(1-4), 3-19, doi:10.1007/s11214-010-9678-3.

Kobayashi, M., N. Hasebe, T. Miyachi*, et al.* (2013), The Kaguya gamma-ray spectrometer: instrumentation and in-flight performances, *Journal of Instrumentation*, *8*(04), P04010, doi:10.1088/1748-0221/8/04/p04010.

Lawrence, D. J., S. Maurice, and W. C. Feldman (2004), Gamma-ray measurements from Lunar Prospector: Time series data reduction for the Gamma-Ray Spectrometer, *JGR*, *109*(E7), doi:10.1029/2003je002206.

Mariscotti, M. A. (1967), A method for automatic identification of peaks in the presence of background and its application to spectrum analysis, *Nuclear Instruments and Methods*, *50*(2), 309-320, doi:10.1016/0029-554X(67)90058-4.

Prettyman, T. H., and W. C. Feldman (2012), PDS data processing Gamma Ray and Neutron Detector. Version 5.1., *NASA Planetary Data System L1A archive*.

Prettyman, T. H., and N. Yamashita (2020), Kaguya Gamma-Ray Spectrometer Ephemerides, Pointing & Geometry Data, *NASA Planetary Data System*, *urn:nasa:pds:kaguya_grs_spectra:document:kgrs_ephemerides_doc*.

Prettyman, T. H., D. Dot Delapp, W. C. Feldman*, et al.* (2004a), Mars 2001 Odyssey Neutron Spectrometer processing. Version 1.3., *NASA Planetary Data System*.

Prettyman, T. H., W. C. Feldman, M. T. Mellon*, et al.* (2004b), Composition and structure of the Martian surface at high southern latitudes from neutron spectroscopy, *109*(E5), E05001.

Prettyman, T. H., W. C. Feldman, H. Y. McSween*, et al.* (2011), Dawn's Gamma Ray and Neutron Detector, *Space Science Reviews*, *163*(1-4), 371-459, doi:10.1007/s11214-011-9862-0.

Yamashita, N., N. Hasebe, R. C. Reedy*, et al.* (2010), Uranium on the Moon: Global distribution and U/Th ratio, *GRL*, *37*, L10201, doi:10.1029/2010gl043061.

Yamashita, N., O. Gasnault, O. Forni*, et al.* (2012), The global distribution of calcium on the Moon: Implications for high-Ca pyroxene in the eastern mare region, *EPSL*, *353-354*, 93-98, doi:10.1016/j.epsl.2012.08.010.